Plasma Chemistry and Plasma Processing
https://doi.org/10.1007/s11090-023-10404-0

ORIGINAL PAPER

# Generation of Multiple Jet Capillaries in Advanced Dielectric Barrier Discharge for Large-Scale Plasma Jets

**Duc Ba Nguyen[1,7] · Shirjana Saud[2] · Quang Thang Trinh[3,4] · Hongjie An[3] · Nam-Trung Nguyen[3] · Hoang Tung Do[5] · Young Sun Mok[2] · Won Gyu Lee[6]**

Received: 31 May 2023 / Accepted: 26 September 2023


## Abstract
A multiple-capillary Ar plasma jet was successfully generated by an advanced dielectric barrier discharge reactor. The reactor consisted of four quartz capillaries arranged separately and covered by two ring-shaped electrodes, which were isolated by a liquid dielectric. The advantages of the reactor included less Ar consumption (ranging from 1 to 3 L/min to obtain a total cross-sectional area of four individual plasma flow components of 3.14 $mm^2$ at the capillary orifices) and low gas temperatures (not exceeding 40 °C). The obtained temperature is suitable for implementing various biomedical applications such as wound healing, dental treatment, and cancer therapy. Furthermore, the plasma jet spread when it interreacted with dielectric materials or skin, resulting in an enlarged effective plasma treatment area of approximately 8 $mm^2$. Analysis of optical emission spectra of the plasma jet indicated the existence of several reactive species, suggesting that the plasma device holds potential for biomedical applications and material surface treatments.

**Keywords** Multi-bore plasma jet · DBD · Ar plasma jet · Cold atmospheric plasma jet

✉ Duc Ba Nguyen
band@plasma.ac.vn

✉ Young Sun Mok
smokie@jejunu.ac.kr

1 Institute of Theoretical and Applied Research, Duy Tan University, Hanoi 100000, Vietnam

2 Department of Chemical Engineering, Jeju National University, Jeju 63243, Republic of Korea

3 Queensland Micro and Nanotechnology Centre, Griffith University, Nathan, QLD 4111, Australia

4 Faculty of Mechanical Engineering, Le Quy Don Technical University, Hanoi, Vietnam

5 International Centre of Physics, Institute of Physics, Vietnam Academy of Science and Technology, 10 Dao Tan, Ba Dinh, Hanoi, Vietnam

6 Division of Chemical Engineering and Bioengineering, Kangwon National University, Chuncheon 24341, Republic of Korea

7 Institute of Research and Development, Duy Tan University, Danang 550000, Vietnam

Published online: 20 October 2023

## Introduction

Recently, there has been a growing interest in cold atmosphere plasma (CAP) sources due to emerging plasma applications such as cancer treatment [1–4], skin treatment [5–8], sterilization [9–12], wound healing [13, 14], and plasma-activated medium [15–18]. In the last two decades, several CAPs have been introduced for these applications in research and commercial products, e.g., plasma pencil and kINPen [19–21]. Besides the general characteristics of CAPs that supply reactive chemical species at low temperatures [17], each plasma source provides unique features. Specifically, the plasma source depends on plasma gas [22, 23], device configurations [24–26], and operating parameters [27, 28]. CAP can be classified into three categories in terms of plasma gas used, namely, noble gas plasma jet, $N_2$ plasma jet, and air plasma jet [29]. Among them, noble gas plasma jets have been more widely used than other plasma jets due to several advantages that noble gas plasma jets such as He or Ar possess. The advantages include low breakdown voltage, long plasma jet, low jet temperature, and stable plasma jet. However, using considerable noble gas flow rates can increase the operating cost of plasma treatment; consequently, less noble gas consumption during plasma is useful for practical applications.

A variety of configurations have been used to generate plasma with noble gases. The four typical configurations include dielectric-free electrode, dielectric barrier discharge (DBD), DBD-like configurations, and single electrode [29]. In terms of avoiding electrical shock and prevention of increasing current during plasma treatment, DBD jets can be considered more suitable than other structures. The reason is that discharge current extinguishes on the dielectric layer surface [30], and high voltage electrodes are isolated with human body parts by strong dielectric layer during direct plasma treatment process. To achieve a large plasma treatment area, a traditional DBD jet typically utilizes a single large-inner-diameter dielectric tube or a bundle of multiple tightly-packed dielectric capillaries [31–33]. Recently, Robert et al. [34, 35] introduced novel methods for converting a single plasma jet to a multi-jet array; herein, multi-plasma jets were generated by extended plasma guns through (i) metallic or dielectric tubes that consisted of up to a hundred hollows with a diameter of 0.5 mm [34] and (ii) a unique outlet part comprising 52 channels with 0.8 mm in diameter [35]. In the case of a single large tube, there should be a large noble gas consumption due to the requirement of a sufficient gas velocity (i.e., the flow rate per cross-section area of the gas flow) to induce an adequate plasma jet length with low temperature. The use of a conventional tightly-packed-capillary type reactor does not significantly reduce the required gas flow rate. If the plasma jet can be generated in the capillaries of a multi-bore dielectric tubing with an appropriate bore distribution, an enlarged treatment surface can be obtained because plasma jets would spread out on the dielectric surface when it touches the treated surface [36–39]. These disadvantages in both single dielectric tubing and narrow array parallel of plasma jets are solved. Moreover, compared to a single dielectric tubing at the same total cross-section tubing area, the capillary surface area of the multi-bore is larger. Indeed, the capillary surface area of a single dielectric tubing is $S_{\text{single}} = \pi l d_{\text{single}}$ (l: length of discharge zone; $d_{\text{single}}$: inner diameter of single dielectric tubing), while the capillary surface area of multi-bore tubing is $S_{\text{bore}} = n\pi l d_{\text{bore}}$ (n: number of bores; $d_{\text{bore}}$: inner diameter of bores). As the cross-section area of the single dielectric tubing equals to that of the multi-bore dielectric tubing, $d_{\text{bore}} = \frac{1}{\sqrt{n}} d_{\text{single}}$. Consequently, $S_{\text{bore}} = \sqrt{n}\pi l d_{\text{single}} = \sqrt{n} S_{\text{single}}$. As a result, the capillary surface area of the multi-bore dielectric tubing is $\sqrt{n}$ times of that with single dielectric tubing. The change of capillary surface area would affect the physical and chemical properties of the plasma jet.

Generation of CAP in a 4-bore tubing was investigated with a noble gas Ar in order to obtain low temperature and long plasma jet targeting the bio-application of plasma. The advanced feature of the 4-bore tubing compared with the traditional single tube was performed and presented. The result indicated that the 4-bore tubing plasma jets have higher performance than that of a single plasma jet in terms of low jet temperature and less gas consumption to obtain the same interaction area between plasma and treated objectives, e.g., glass materials, $CaF_2$, human skin, etc. Furthermore, the effective plasma of 4-bore plasma jets is also higher than that of the single plasma jet.

## Experimental

In this work, multiple plasma jets were generated by an advanced DBD plasma jet, which comprised several plasma jet capillaries created by using 4-bore dielectric tubing instead of single dielectric tubing in the DBD reactor configuration, as shown in Fig. 1. The reactor consists of two ring-shaped electrodes (thickness of 0.5 mm) covering the 4-bore quartz tubing (bore diameters of 1 mm; outer diameter of 6 mm) and the electrodes were isolated with the atmosphere by immersing liquid dielectric (KS C2301, Michang Oil, Korea). The

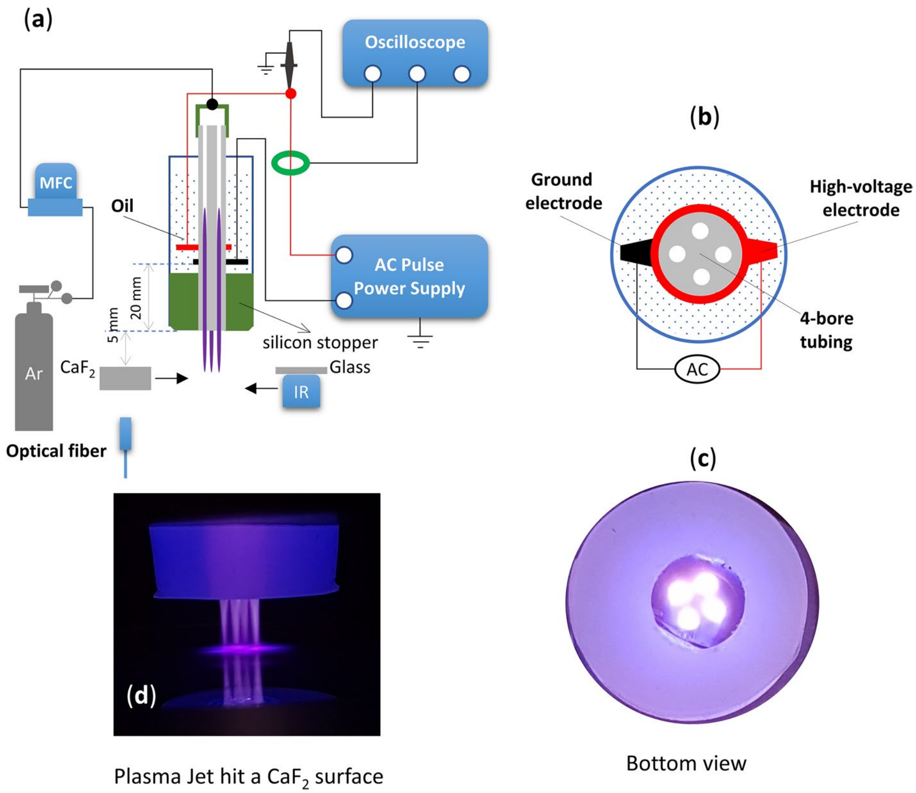


**Fig. 1** **a** schematic diagram of experimental setup, **b** cross-section of the reactor, **c** photo of bottom view of plasma jet, and **d** side view of plasma jet hit a $CaF_2$ surface

distance between the two electrodes was fixed at 6 mm; the distance from the orifices of the quartz tube to the lower grounded electrode was fixed at 20 mm. Ar gas with a purity of 99.999% was introduced to the reactor by a mass flow controller (MFC).

The jet capillaries were driven by an AC pulse power supply (AP Plasma Power Supply, HVP, Korea), which supplied AC microsecond voltage pulses with a 30 kHz frequency [28]. The power can be supplied with the maximum voltage and power up to 15 kV and 2 kVA, respectively, with 1.25 μs rise time for voltage from 0 to 15 kV at a frequency of 30 kHz. Electrical data during plasma jet generation were recorded by a digital oscilloscope (Tektronix, DPO 3034, four channels, 300 MHz, 2.5 GS/s, USA). Herein, the high voltage was measured via a passive high voltage probe (Tektronix, P6015A, 75 MHz, USA), while the current was monitored with a current monitor (Pearson Electronics, 2100, 20 MHz, USA). Consequently, the electrical measure system is compatible with recording the micro-pulse signal. The discharge power (P) delivered to the capillaries was estimated by integrating instantaneous voltage and the current measured on the high voltage wire [40]. Several parameters of the plasma jet were determined, namely: jet length, jet temperature, and optical emission spectra. The jet length was determined by a ruler placed parallel to the plasma jet axis, with an error margin of $\pm 1$ mm. The jet temperature was determined through a balanced temperature of glass slide over an infrared thermometer (IRtech, IR4, Korea; Repeatability: ±1 °C, D:S target ratio: 12:1). Specifically, the infrared tip was covered by a 1-mm-thick glass slide (Microscope slides, Marienfeld, Germany), one side touched the tip. The tip was placed at the jet axes and fixed at the distance from the nozzle exits to the up-side glass was 5 mm, as shown in Fig. 1a. The plasma jet interacted with the glass slide, when the infrared thermometer monitor obtained a stable temperature, denoted as a jet temperature for these conditions; the interaction time requirement was at least 5 min for the stable temperature. Optical emission of the plasma jet was recorded by an optical emission spectrometer (OES, AvaSpec-2048 XL, Netherlands). Herein, to facilitate the measurement of optical emission spectra, a 4-mm-thick polished $CaF_2$ window was located between the nozzle exits and the tip of the optical fiber, with a distance from the nozzle exits and tip to each side of $CaF_2$ was 5 and 10 mm, respectively. The plasma-induced, long-lived species from the plasma jet were detected using a portable gas analyzer (Ecom® EN2, ecom GmbH, Germany) with a total of 1.5 L/min of the gas samples. The gas samples were collected by a cone glass funnel with the tube connected to the inlet of the 1.5 L/min gas pump. To create open space, the funnel has a diameter larger than the body reactor; it is located downstream with the plasma jets inside the cone funnel. The top or cross-sectional view of the multi-bore jet is shown in Fig. 1b. The photos of multiple gas discharges with bottom and side view are shown in Fig. 1c and d, respectively. Figure 1d indicated that when jet capillaries hit $CaF_2$ surface (dielectric material), plasma jets spread on the surface, getting more effective area (up to a square of $\sqrt{8}$, i.e., 8 $mm^2$); this area is superior to a 2 mm diameter circle (π $mm^2$), which is the diameter of single-bore dielectric tubing with an equal total cross-section to the 4-bore dielectric tubing.

## Results and Discussion

### Electrical Properties of the Plasma Jets

The multiple gas discharges were driven by an AC voltage pulse, as shown in Fig. 2a. Each voltage phase has 3 major pulses with a total pulse width of 7 μs. The first pulse voltage

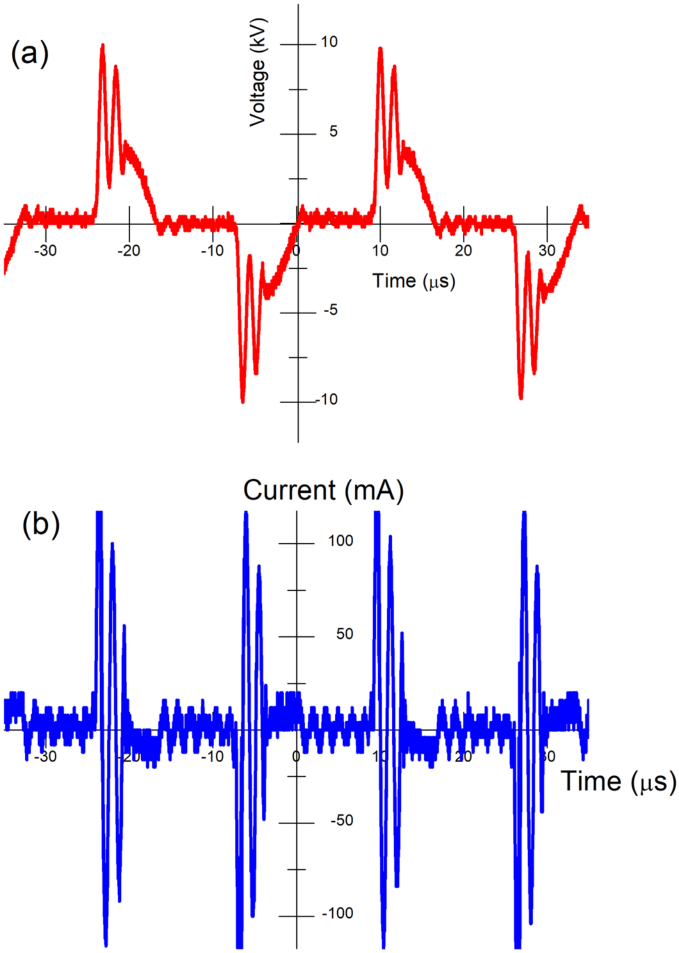


**Fig. 2** Voltage waveforms (**a**) and current discharge (**b**) under applied voltage of 10 kV, frequency of 30 kHz, and Ar flow rate of 2 L/min

had high intensity, and immediately voltage rose to the amplitude value within approximately 1.0 μs and a pulse width of 1.75 μs; the second pulse maintained a pulse width of 1.75 μs, but the voltage intensity gradually decreased. In contrast with the third pulse, both intensity and rising rate of voltage decreased (pulse width of 3.5 μs and voltage intensity decreased to zero). In response to varying voltage, the current had 5 major pulses with a total pulse width of 3.5 μs for each voltage phase, and the current intensity decreased correspondingly to the decreasing intensity of the voltage pulse. As a result, the maximum intensity of the current pulse was around 100 mA level.

The effect of applied voltage and Ar flow rate on the generation of plasma discharge was observed, as depicted in Fig. 3. It can be observed that with an increase in applied voltage, the discharge power increases slightly, whereas the discharge power shows the opposite trend with an increase in Ar flow rate (i.e., reduced discharge power). The increased applied voltage raises the energy/density of electrons [41, 42] and/or excited/metastable species [43] in the plasma zone and may increase the amount of charge transfer owing to

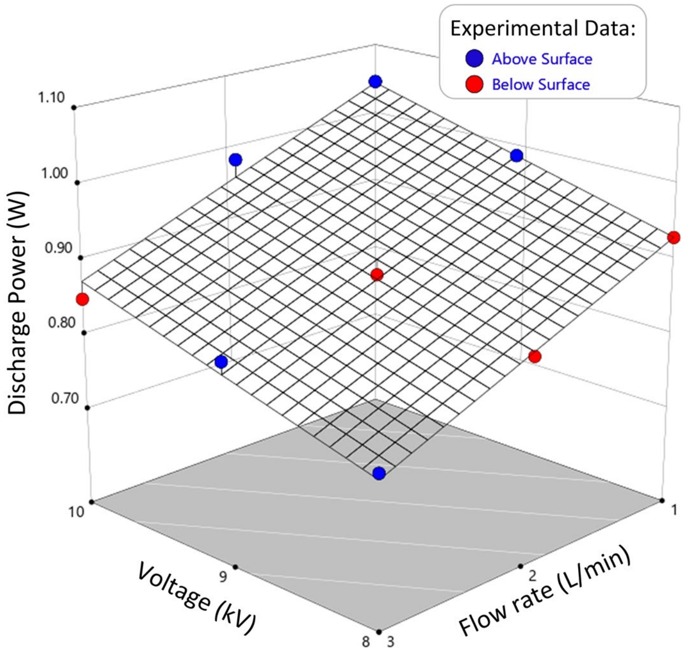


**Fig. 3** Discharge power under various voltage and Ar flow rate (experimental data point: average of 128 samples with a standard deviation for each discharge power point from 0.230 to 0.370 W; above surface: experimental data ≥ estimated data; below surface: experimental data ≤ estimated data, estimated data are calculated at the same input parameters by the linear model)

the enhanced electric field across the electrodes, which is one of the key factors in enhancing the discharge power. However, the discharge power decreases ~ 17% on average when the Ar flow rate increases from 1 to 3 L/min, which can be attributed to reduced retention time in the discharge zone due to increased gas velocity from 5.3 to 15.9 m/s, respectively.

Since an AC voltage pulse drives the plasma jet, the current discharge has high intensity and short pulse width, suggesting enlarging instantaneous power that the plasma jet source can provide. Indeed, the discharge power can be calculated by $P(W) = f\int_0^T V_t I_t dt$ [25]. Therefore, compared with a sinusoidal waveform, high instantaneous power is observed for a pulse waveform at a similar range of discharge power under the same frequency and voltage amplitude [44]. In other words, large current discharge intensities for shorter pulses resulted in more electron production and potential high electron density. Zhang et al. [45] compared microsecond pulse with nanosecond pulse for the He plasma jet. The results indicated that a nanosecond pulse was a cause of high discharge current, longer plasma jet, and stronger spectral line intensity; these results supported the above hypothesis. Moreover, with a short width pulse time, the discharge power deposited into the discharge zone will be less [45]; consequently, the gas temperature, due to heating during plasma discharge, after plasma discharge is not high. Indeed, the discharge power under varying applied voltage and Ar flow rate was in the range of 0.77 to 1.05 W. The specific heat capacity of Ar in the atmospheric pressure is around $C_p = 20.8$ J/mol K [46]; consequently, the highest increase of gas temperature during plasma is not over 73 K ($\Delta T \leq \frac{P*60}{C_p*\frac{F}{24.4}} = \frac{1.05*60}{20.8*\frac{1}{24.4}} = 73\,\mathrm{K}$ ; P(W): discharge power; F(L/min): Ar flow rate, volume of 1 mol gas at 25 °C is 24.4 L). The plasma jet was performed under atmospheric conditions (~25 °C). Thus, the Ar gas temperature through the orifices of the quartz tube will be estimated not over 98 °C (25+73 °C), suggesting low-temperature plasma can be obtained by the 4-bore DBD plasma jet.

## Plasma Jet Performance Under Different Voltages and Flow Rates

Even though the Ar flow rate had a negative effect on the discharge power, the flow rate and applied voltage both positively influenced the plasma jet length, as presented in Fig. 4a. In Fig. 4, the above and below surface points represent the experimental data higher and lower than that of anticipated data by the quadratic or linear model, respectively. These models resulted from fitting experimental data with a desirable $R^2 \geq 0.95$. The fitting data were carried out by the Design Expert tool (version 12); actual equations with V (applied voltage) and F (flow rate) are independent variables given below:

Jet length(mm) $= -48.5 + 10.33\text{V} - 0.42\text{F} + 0.75\text{VF} - 0.5\text{V}^2 - 1.0\text{F}^2 (R^2 = 0.995)$.

Jet temperature(°C) $= 13.6 + 3.03\text{V} - 4.02\text{F} \left(R^2 = 0.957\right)$.

The minimum plasma jet length was observed to be 7 mm at [flow rate (L/min), applied voltage (kV)] = [1, 8], and the maximum jet length was acquired to be 17 mm at [flow rate (L/min), applied voltage(kV)] = [3, 10]. Although increased applied voltage contributes to the enhancement of jet length, a part of the input energy is spent on heating the discharge gas as well as the reactor, resulting in variation of jet temperature with respect to input parameters. Herein, with increased applied voltage, more energy is input to the system, as evident by increased discharge power in Fig. 3, which results in the jet temperature elevation, as presented in Fig. 4b. However, with an increment in flow rate, the jet temperature displayed a reduced tendency. That is, the increased flow rate, meaning increased gas volume (amount), significantly reduced the changed temperature ($\Delta\text{T} = \frac{E\left(\frac{J}{\text{min}}\right)}{C_p\left(\frac{J}{\text{mol}.K}\right) * \frac{F\left(\frac{L}{\text{min}}\right)}{\frac{24.4L}{\text{mol}}}}$; E is

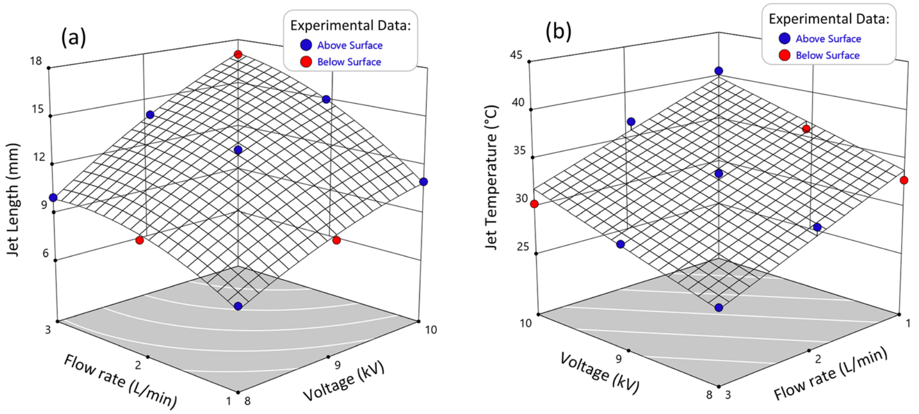


**Fig. 4** Dependence of plasma jet on applied voltage and flow rate (experimental data point was the average of 3 samples with the standard error of length and temperature measurement of ±1 mm and 1 °C, respectively; above surface: experimental data ≥ estimated data; below surface: experimental data ≤ estimated data, estimated data are calculated at the same input parameters by the models, the quadratic model for jet length while jet temperature by the linear model)

part of the input energy for heating gas), resulting in the reduced jet temperature. Furthermore, at high velocity, it works like a functional cooling system. Particularly, a minimum jet temperature of 26 °C was observed at a combination of 3 L/min Ar flow rate and 8 kV applied voltage, whereas a maximum jet temperature of 40.6 °C was seen at a combination of 1 L/min Ar flow rate and 10 kV applied voltage, which is way below the highest possible overall temperature of 98 °C during plasma generation with Ar as the discharge gas. This can be explained by input energy (discharge power) being used not only to heat gas but also to create energetic electrons, ions, radicals, excited species, photons, etc., heating other reactor parts [47, 48]. While the plasma plume moves from the discharge zone to reach the glass slide, there is an energy transfer from the Ar flow to the reactor body and ambient air, which is also a reason for the low-temperature plasma jet.

## Optical Emission Spectra

The optical emission spectra of multiple plasma jet was plotted in Fig. 5. The spectra indicated a strong emission of Ar plasma was obtained by the 4-bore DBD plasma jet. Indeed, the intensities of Ar lines (for instance, 696.5, 763.5, 772.3, 826.5 nm) in this work are much higher than in the previous report [49] with the same typical applied voltage, i.e., these intensities increased around 1.5 times. Furthermore, by the method of the plasma jet interacting with the $CaF_2$ surface and the tip of the optical fiber located at another the $CaF_2$ window side, it is more accessible to carry out optical emission spectra recording than the usual way [25]. The spectra of the 4-Ar plasma jet consisted of main Ar lines ranging from 690 to 900 nm and merge lines of OH and $N_2$ at 308 with high intensity, overall higher than $10^4$ a.u. intensity. During the propagation of the plasma jet into the atmosphere, Ar plasma jet interacted with ambient air, resulting in several excited active species; they are

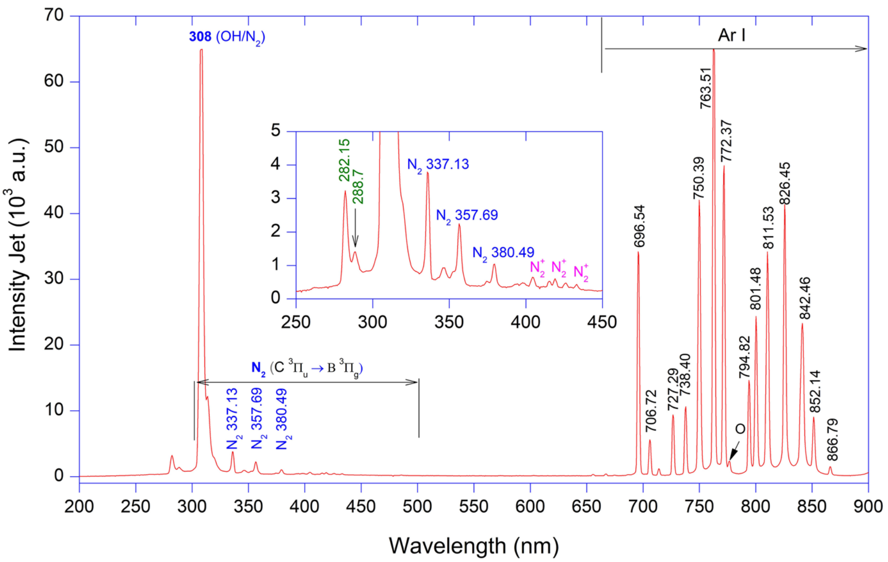


**Fig. 5** Optical emission spectra of the multiple jet capillaries at 10 kVp (applied frequency = 30 kHz; Ar flow rate = 2 L/min; spectra: averaging 50 scans)

represented through several intense peaks in the spectra, e.g., $N_2$, $N_2^+$, O, and OH. Strong lines of $N_2$ in the second positive system ($C^3\Pi_u \rightarrow B^3\Pi g$) were observed in the range from 300 to 500 nm, while the emission of $N_2^+$ in the first negative system ($B^2\Sigma_u^+ \rightarrow X^2\Sigma_g^+$) was also detected in the range wavelength from 380 to 450 nm, as shown in the inset figure. The atomic oxygen was indicated by a peak at 777 nm. Interestingly, no clear NO lines were detected in the $A^2\Sigma^+ \rightarrow X^2\Pi$ system with a wavelength from 200 to 300 nm, which agreed with no $NO_x$ detected by the $NO_x$ analyzer, as shown below. To summarize, analysis of the 4-bore DBD plasma jet spectra demonstrated high intensities of emission of excited species. In other words, the plasma provides a source of activated gas fluid at close room temperatures (~40 °C), proposing potential applications in bio-applications and material treatment, particularly for sensitive materials that are susceptible to high temperatures or chemical agents.

## Emission of $O_3$ and $NO_x$

To practically apply the plasma jet as a potential plasma source in the bio application field, it is desired to have low to no hazardous chemical emissions [such as $O_3$, $NO_x$ (NO and $NO_2$)] when the plasma jet interacts with ambient air. The emission of $O_3$ and $NO_x$, when the plasma jet was exposed to ambient air, was examined at a maintained flow rate of 2 L/min by varying the applied voltage from 8 to 12 kV. The threshold limit of $O_3$, NO, and $NO_2$ that would not adversely affect humans upon exposure is 0.1, 25, and 0.2 ppm, respectively [50]. Figure 6 shows the gas emitted and its concentration; herein, no $NO_x$ was detected under the experimental conditions. However, around 0.3 ppm of $O_3$ was observed at an applied voltage of 12 kV, which does not significantly surpass the limits, considering the possibility of dilution and decomposition to $O_2$ [51]. Notably, $O_3$ was under the threshold limit, and no $NO_x$ was detected at an applied voltage $\leq$ 10 kV.

## Plasma Jet Features/Pattern when it Interacts with Human Skin

The results of the plasma jet length, temperature, and chemical compositions from the previous section demonstrate the potential of the multi-capillary plasma jet generated in this work for biomedical applications. In order to intuitively show its capability, a test of the plasma jet interacting with human skin was conducted and illustrated in Fig. 7. It can be seen that the plasma jet length was poor without a finger at an applied voltage of 8 kV and flow rate of 2 L/min. Under these conditions, no hazardous gas was emitted, and the plasma jet temperature was about 30.7 °C, less than the body temperature, which is ideal for bio-applications such as skin treatment, cancer treatment, sterilization, and wound

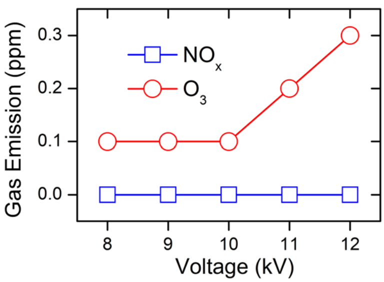


**Fig. 6** Emission of $NO_x$ and $O_3$ during plasma treatment (applied frequency = 30 kHz; Ar flow rate = 2 L/min)

**Fig. 7** Effect of human skin on exhibited plasma jet (applied voltage = 8 kV; Ar flow rate = 2 L/min)

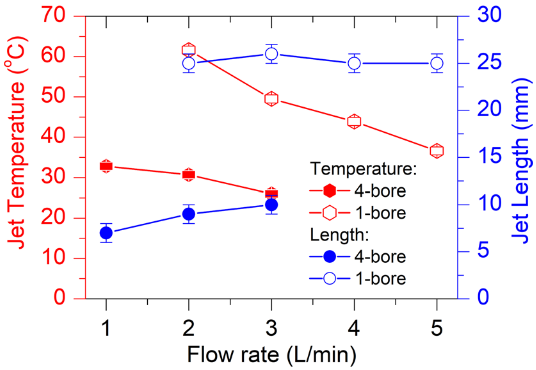


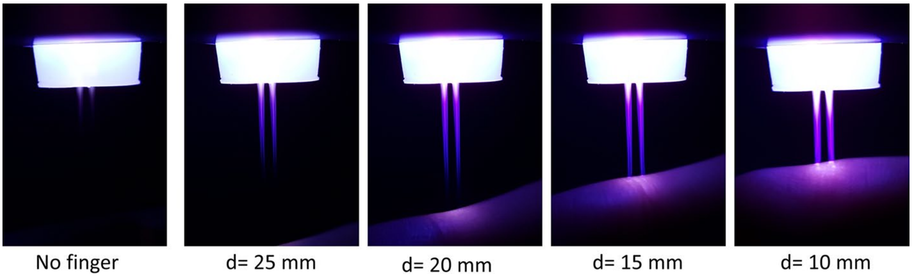


**Fig. 8** A comparison between 1-bore and 4-bore plasma jet performance (applied voltage = 8 kV; applied frequency = 30 kHz; total cross-section of bores is π $mm^2$; the lengths of electrodes are different in the two reactors)

healing. With the introduction of a human finger in the scenario at a proximity of 25 mm, a visible improvement in the jet length and intensity was observed, which was further enhanced when the finger was placed closer and closer to the reactor outlet. This phenomenon can be attributed to the finger acting as a floating ground that helps channel the plasma jet, improving the jet length and intensity [25]. The results are in agreement with those obtained by Robert et al. [52, 53]; plasma propagation depended on the nature of the target (electrical conductivity) [52], and helium metastable production increased both inside the capillary and plasma plume with conductive targets [53]. The results also suggest that the visible optical jet length strongly depended on the surrounding environment of the plasma jet, especially when the plasma jet interacted with an object that can function as a floating electrode.

## Comparison Between a 1-Bore and 4-Bore Configuration for Plasma jet Performance

A comparison between plasma jet generation by 1-bore and 4-bore plasma jet was performed and shown in Fig. 8. The comparison was based on the same total cross-section of bores and applied voltage. The data of the 1-bore plasma jet was taken from the previous report [49]. The 1-bore reactor also had a similar DBD configuration. Here, it should be noted that the 1-bore reactor has longer electrodes than 4-bore reactor and a different shape dielectric tube. Specifically, the power and ground electrode lengths are

20 mm and 5 mm, respectively, whereas both electrodes are 0.5 mm for the 4-bore reactor. The plasma jet was generated in a quartz tube with an inner diameter of 2 mm and outer diameter of 4 mm. Consequently, 1-bore plasma also had a cross-section bore area of $\pi$ mm$^2$, which equals to total cross-section bore area in the 4-bore plasma jet. The same applied voltage of 8 kV at 30 kHz was supplied to these reactors for the generation of the plasma jet. The figure demonstrated a significant decrease in jet temperature and Ar consumption for the 4-bore plasma jet case. Particularly, the Ar consumption by 4-bore plasma ranges from 1 to 3 L/min to achieve a jet temperature below 40 °C. On the other hand, the 1-bore plasma jet required up to 5 L/min of Ar flow rate to obtain a plasma jet temperature $\leq$ 40 °C. A plausible reason for this is the low discharge powers in 4-bore plasma jet (at 1.0 W level). However, under the same conditions, the jet length of the 1-bore plasma jet is longer than that of the 4-bore plasma jet; although a shorter jet length of the 4-bore plasma jet, its length is still suitable for the applications.

## Conclusions

This work investigated the generation of multiple jet capillaries using a DBD configuration. For this purpose, a modified DBD configuration was employed, wherein the reactor consisted of two ring-shaped electrodes that covered the 4-bore quartz tubing, with the electrodes immersed in a liquid dielectric. The plasma jet was driven by a µs pulse of AC high voltage, resulting in low gas temperature due to the small electrical power deposited into the discharge. By utilizing 4-bore tubing instead of single-bore tubing as the dielectric layer in DBD plasma jet configuration, the reactor exhibited high-performance plasma jet generation, characterized by reduced Ar consumption, low-temperature plasma jet, and a large surface area for plasma jet effects, compared to a single-bore tubing with the same cross-section area. Additionally, the visible jet length of the multiple jet capillaries was found to be strongly influenced by the distance between the finger and the nozzle exits. The multiple jet capillaries offer reactivated chemical sources at temperatures below 40 °C and hold potential for plasma bio-applications.

**Author Contributions** DBN: Conceptualization, Methodology, Investigation, Writing - Original Draft, Writing - Review & Editing; SS: Investigation, Writing - Original Draft, Writing - Review & Editing; QTT, HA, N-TN, QHT, HTD, and WGL: Participated in the interpretation of the results, Investigation, Writing - Review & Editing; YSM: Supervision, Writing - Review & Editing, Funding acquisition.

**Funding** This work was supported by the Basic Science Research Program through the National Research Foundation funded by the Korean government (MSIT) (2021R1A2C2011441 & 2021R1A4A2000934).

**Data Availability** Not applicable.

## Declarations

**Conflict of interest** The authors declare no conflict of interest.

**Ethical Approval** Not applicable.

## References


1. Poramapijitwat P, Thana P, Sukum P, Liangdeng Y, Kuensaen C, Boonyawan D (2023) Selective cytotoxicity of lung cancer cells—A549 and H1299—Induced by ringer's lactate solution activated by a non-thermal air plasma jet device, Nightingale®. Plasma Chem Plasma Process 43:805–830
2. Chaturvedi Misra V, Pai BG, Tiwari N, Patro BS, Ghorui S (2023) Excitation frequency effect on breast cancer cell death by atmospheric pressure cold plasma. Plasma Chem Plasma Process 43:467–490
3. Vandamme M, Robert E, Pesnel S, Barbosa E, Dozias S, Sobilo J, Lerondel S, Le Pape A, Pouvesle J-M (2010) Antitumor Effect of plasma treatment on U87 glioma xenografts: preliminary results. Plasma Process Polym 7:264–273
4. Lu X, Bruggeman PJ, Reuter S, Naidis G, Bogaerts A, Laroussi M, Keidar M, Robert E, Pouvesle J-M, Liu D, Ostrikov K (2022) Grand challenges in low temperature plasmas. Frontiers Phys 10:109
5. Vijayarangan V, Dozias S, Heusèle C, Jeanneton O, Nizard C, Pichon C, Pouvesle JM, Stancampiano A, Robert E (2023) Boost of cosmetic active ingredient penetration triggered and controlled by the delivery of kHz plasma jet on human skin explants. Front Phys 11:285
6. Busco G, Robert E, Chettouh-Hammas N, Pouvesle J-M, Grillon C (2020) The emerging potential of cold atmospheric plasma in skin biology. Free Radical Biol Med 161:290–304
7. Dubey SK, Parab S, Alexander A, Agrawal M, Achalla VPK, Pal UN, Pandey MM, Kesharwani P (2022) Cold atmospheric plasma therapy in wound healing. Process Biochem 112:112–123
8. Lu X, Reuter S, Laroussi M, Liu D (2019) Nonequilibrium Atmospheric pressure plasma jets. CRC Press, Boca Raton
9. Muto R, Hayashi N (2023) Sterilization characteristics of narrow tubing by nitrogen oxides generated in atmospheric pressure air plasma. Sci Rep 13:6947
10. Shaw P, Kumar N, Kwak HS, Park JH, Uhm HS, Bogaerts A, Choi EH, Attri P (2018) Bacterial inactivation by plasma treated water enhanced by reactive nitrogen species. Sci Rep 8:11268
11. Attri P, Han J, Choi S, Choi EH, Bogaerts A, Lee W (2018) CAP modifies the structure of a model protein from thermophilic bacteria: mechanisms of CAP-mediated inactivation. Sci Rep 8:10218
12. Kelar Tučeková Z, Vacek L, Krumpolec R, Kelar J, Zemánek M, Černák M, Růžička F (2021) Multi-hollow surface dielectric barrier discharge for bacterial biofilm decontamination. Molecules 26:910
13. Weltmann KD, von Woedtke T (2016) Plasma medicine—current state of research and medical application. Plasma Phys Controlled Fusion 59:014031
14. Yusupov M, Lackmann J-W, Razzokov J, Kumar S, Stapelmann K, Bogaerts A (2018) Impact of plasma oxidation on structural features of human epidermal growth factor. Plasma Process Polym 15:1800022
15. Pastorek M, Suchoňová M, Konečná B, Pásztor S, Petrus J, Ivašková N, Celec P, Gardlík R, Machala Z, Tóthová Ľ (2022) The effect of air plasma activated liquid on uropathogenic bacteria. Plasma Chem Plasma Process 42:561–574
16. Laroussi M, Bekeschus S, Keidar M, Bogaerts A, Fridman A, Lu X, Kostya, Ostrikov, Hori M, Stapelmann K, Miller V, Reuter S, Laux C, Mesbah A, Walsh J, Jiang C, Thagard S, Tanaka H, Liu D, Yusupov M (2021) Low temperature plasma for Biology. Perspective and Roadmap, Hygiene, and Medicine
17. von Woedtke T, Laroussi M, Gherardi M (2022) Foundations of plasmas for medical applications. Plasma Sources Sci Technol 31:054002
18. Li Y, Nie L, Liu D, Kim S, Lu X (2022) Plasma-activated chemical solutions and their bactericidal effects. Plasma Process Polym 19:2100248
19. Laroussi M, Lu X (2005) Room-temperature atmospheric pressure plasma plume for biomedical applications. Appl Phys Lett 87:113902
20. Winter J, Brandenburg R, Weltmann KD (2015) Atmospheric pressure plasma jets: an overview of devices and new directions. Plasma Sources Sci Technol 24:064001
21. Reuter S, Woedtke TV, Weltmann K-D (2018) The kINPen—a review on physics and chemistry of the atmospheric pressure plasma jet and its applications. J Phys D Appl Phys 51:233001
22. Kapaldo J, Han X, Ptasinska S (2019) Shielding-gas-controlled atmospheric pressure plasma jets: optical emission, reactive oxygen species, and the effect on cancer cells. Plasma Process Polym 16:1800169
23. Narimisa M, Onyshchenko Y, Van Rooij O, Morent R, Sobota A, De Geyter N (2022) A poly-diagnostic study of the shield gas-assisted atmospheric pressure plasma jet propagation upon a dielectric surface. Plasma Process Polym 19:2100247
24. Adress W, Graham WG (2022) Comparison study of two atmospheric pressure plasma jet configurations for plasma-catalyst development. Plasma Chem Plasma Process 42:1329–1344

25. Nguyen DB, Trinh QH, Mok YS, Lee WG (2020) Generation of cold atmospheric plasma jet by a coaxial double dielectric barrier reactor. Plasma Sources Sci Technol 29:035014
26. Bekeschus S, Lin A, Fridman A, Wende K, Weltmann K-D, Miller V (2018) A comparison of floating-electrode DBD and kINPen jet: plasma parameters to achieve similar growth reduction in colon cancer cells under standardized conditions. Plasma Chem Plasma Process 38:1–12
27. Wang J, Wang T, Wang X, Yang W, Wang Z, Li M, Shi L (2023) Effect of applied voltage on localized deposition of silicon dioxide-like films on stainless steel using atmospheric pressure microplasma jet. Plasma Chem Plasma Process 43:879–899
28. Nguyen DB, Mok YS, Lee WG (2019) Enhanced atmospheric pressure plasma jet performance by an alternative dielectric barrier discharge configuration. IEEE Trans Plasma Sci 47:4795–4801
29. Lu X, Laroussi M, Puech V (2012) On atmospheric-pressure non-equilibrium plasma jets and plasma bullets. Plasma Sources Sci Technol 21:034005
30. Kogelschatz U (2003) Dielectric-barrier discharges: their history, discharge physics, and industrial applications. Plasma Chem Plasma Process 23:1–46
31. Ren Q, Liu X, Sun H, Huang C, Zhou F, Chen M, Liang C (2020) XJTU: typical arrangements for downstream uniformity assessment in atmospheric-pressure plasma jet arrays. IEEE Access 8:92945–92953
32. Xia Y, Wang W, Liu D, Peng Y, Song Y, Ji L, Zhao Y, Qi Z, Wang X, Li B (2017) An atmospheric-pressure microplasma array produced by using graphite coating electrodes. Plasma Process Polym 14:1600132
33. Qian C, Fang Z, Yang J, Kang M (2014) Investigation on atmospheric pressure plasma jet array in ar. IEEE Trans Plasma Sci 42:2438–2439
34. Robert E, Darny T, Dozias S, Iseni S, Pouvesle JM (2015) New insights on the propagation of pulsed atmospheric plasma streams: from single jet to multi jet arrays. Phys Plasmas 22:12
35. Maho T, Binois R, Brulé-Morabito F, Demasure M, Douat C, Dozias S, Escot Bocanegra P, Goard I, Hocqueloux L, Le Helloco C, Orel I, Pouvesle J-M, Prazuck T, Stancampiano A, Tocaben C, Robert E (2021) Anti-bacterial action of plasma multi-jets in the context of chronic wound healing. Appl Sci 11:9598
36. Butterworth T, Allen RWK (2017) Plasma-catalyst interaction studied in a single pellet DBD reactor: dielectric constant effect on plasma dynamics. Plasma Sources Sci Technol 26:065008
37. Sobota A, Guaitella O, Sretenović GB, Kovačević VV, Slikboer E, Krstić IB, Obradović BM, Kuraica MM (2019) Plasma-surface interaction: dielectric and metallic targets and their influence on the electric field profile in a kHz AC-driven he plasma jet. Plasma Sources Sci Technol 28:045003
38. Viegas P, Slikboer E, Bonaventura Z, Guaitella O, Sobota A, Bourdon A (2022) Physics of plasma jets and interaction with surfaces: review on modelling and experiments. Plasma Sou Sci Technol 31:053001
39. Slikboer E, Guaitella O, Garcia-Caurel E, Sobota A (2022) Towards plasma jet controlled charging of a dielectric target at grounded, biased, and floating potential. Sci Rep 12:1157
40. Nguyen DB, Trinh QH, Hossain MM, Lee WG, Mok YS (2019) Improvement of electrical measurement of a dielectric barrier discharge plasma jet. IEEE Trans Plasma Sci 47:2004–2010
41. Dong L, Ran J, Mao Z (2005) Direct measurement of electron density in microdischarge at atmospheric pressure by stark broadening. Appl Phys Lett 86:16
42. Hong Y, Niu J, Pan J, Bi Z, Ni W, Liu D, Li J, Wu Y (2016) Electron temperature and density measurement of a dielectric barrier discharge argon plasma generated with tube-to-plate electrodes in water. Vacuum 130:130–136
43. Jo A, Joh HM, Chung JW, Chung TH (2020) Cell viability and measurement of reactive species in gas- and liquid-phase exposed by a microwave-excited atmospheric pressure argon plasma jet. Curr Appl Phys 20:562–571
44. Nguyen DB, Lee WG (2015) Comparison of different applied voltage waveforms on $CO_2$ reforming of $CH_4$ in an atmospheric plasma system. Korean J Chem Eng 32:62–67
45. Zhang C, Shao T, Wang R, Zhou Z, Zhou Y, Yan P (2014) A comparison between characteristics of atmospheric-pressure plasma jets sustained by nanosecond- and microsecond-pulse generators in helium. Phys Plasmas 21:10
46. Prudich ME, Chen H, Gu T, Gupta RB, Johnston KP, Lutz H, Ma G, Su Z (2008) Perry's chemical engineers' handbook, section 2 physical and chemical data. McGraw-Hill Publishing
47. Nozaki T, Miyazaki Y, Unno Y, Okazaki K (2001) Energy distribution and heat transfer mechanisms in atmospheric pressure non-equilibrium plasmas. J Phys D Appl Phys 34:3383–3390
48. Villarreal-Medina R, Murphy AB, Méndez PF, Ramírez-Argáez MA (2023) Heat transfer mechanisms in arcs of various gases at atmospheric pressure. Plasma Chem Plasma Process 43:787–803

49. Nguyen DB, Trinh QH, Lee WG, Mok YS (2019) Analysis of an ar plasma jet in a dielectric barrier discharge conjugated with a microsecond pulse. Plasma Sci Technol 21:095401
50. Haynes WM (ed) (2016) CRC handbook of chemistry and physics, 96th edition (Internet Version 2016). CRC Press/Taylor and Francis, Boca Raton, FL, p 186
51. Saud S, Nguyen DB, Bhattarai RM, Matyakubov N, Nguyen VT, Ryu S, Jeon H, Kim SB, Mok YS (2022) Plasma-catalytic ethylene removal by a ZSM-5 washcoat honeycomb monolith impregnated with palladium. J Hazard Mater 426:127843
52. Riès D, Dilecce G, Robert E, Ambrico PF, Dozias S, Pouvesle JM (2014) LIF and fast imaging plasma jet characterization relevant for NTP biomedical applications. J Phys D Appl Phys 47:275401
53. Darny T, Pouvesle JM, Puech V, Douat C, Dozias S, Robert E (2017) Analysis of conductive target influence in plasma jet experiments through helium metastable and electric field measurements. Plasma Sources Sci Technol 26:045008